PCCP

Accepted Manuscript

ROYAL SOCIETY OF CHEMISTRY

www.rsc.org/pccp

ZnO Modified ZSM-5 and Y Zeolites Fabricated by Atomic Layer Deposition for Propane Conversion

Ting Gong, Lijun Qin, Jian Lu, and Hao Feng*
Xi'an Modern Chemistry Research Institute, Xi'an, Shaanxi, 710065, China
* Corresponding author
Hao Feng: fenghao98@hotmail.com

Abstract

ZnO modified ZSM-5 and Y zeolites are synthesized by performing atomic layer deposition (ALD) of ZnO to HZSM-5 and HY using diethylzinc and water as the precursors. The surface area and pore volume of ZSM-5 and Y zeolites are progressively reduced with the increasing number of ZnO ALD cycle. XRD and SEM characterizations show that highly dispersed ZnO species are deposited on the internal and external surfaces of both zeolites. The ZnO species deposited on ZSM-5 are in an amorphous form while nano-crystallites of ZnO are present on Y zeolite after performing $\geqslant$2 cycles of ZnO ALD. XPS and TPR characterizations reveal that isolated $Zn(OH)^+$ species are predominantly formed on both zeolites after the first cycle of ZnO ALD and the ZnO clusters gradually grow larger with the increasing number of ALD cycle. The type and strength of acid sites on the parent and the ALD ZnO modified zeolites are studied by FTIR spectra of adsorbed pyridine. Incorporation of ZnO to Y zeolite by ALD completely eliminates the Brønsted acid sites and increases the number of strong Lewis acid sites. Similar effects are obtained on ALD ZnO modified ZSM-5 except that the Brønsted acid sites are only partially removed. Catalytic properties of the ALD ZnO modified zeolites are evaluated in propane conversion. Introduction of ZnO species significantly improves the activities of both zeolites. Propylene is the major reaction product on ALD ZnO modified Y zeolite while high selectivities to aromatics are achieved on ALD ZnO modified ZSM-5. These results suggest that ZnO species merely promote the dehydrogenation reaction while the subsequent oligomerization and cyclization reactions require Brønsted acid sites. For both zeolites the catalyst fabricated by only 1 or 2 cycles of ZnO ALD performs better than those fabricated by multiple cycles of ALD, indicating that isolated $Zn(OH)^+$ species are more effective for the conversion of propane to propylene and aromatics.

Keywords

Atomic layer deposition (ALD); Zinc oxides (ZnO); ZSM-5; Y zeolite; propane.

Nomenclature

AAO	Anodic aluminum oxide
ALD	Atomic layer deposition

BAS	Brønsted acid sites
BE	Binding energy
BET	Brunauer-Emmett-Teller
BTX	Benzene, Toluene, Xylene
CVD	Chemical vapor deposition
DEZ	Diethyl Zinc
EDX	Energy dispersive X-ray spectrometer
FID	Flame ionized detector
GC	Gas chromatography
ICP-AES	Inductively coupled plasma atomic emission spectrometer
IE	Ion exchange
IWI	Incipient wetness impregnation
LAS	Lewis acid sites
ODH	Oxidative dehydrogenation
Py-IR	Pyridine adsorption Fourier-transform infrared spectroscopy
sccm	standard cubic centimeter per minute
SEM	Scanning electron Microscopy
TCD	Thermal conductivity detactor
TGA	Thermogravimetric analysis
TPR	Temperature-programmed reduction
USY	Ultra stable Y (zeolite)
WHSV	Weight hourly space velocity
XPS	X-ray photoelectron spectroscopy
XRD	X-ray Diffraction

Table of contents (graphic abstract)

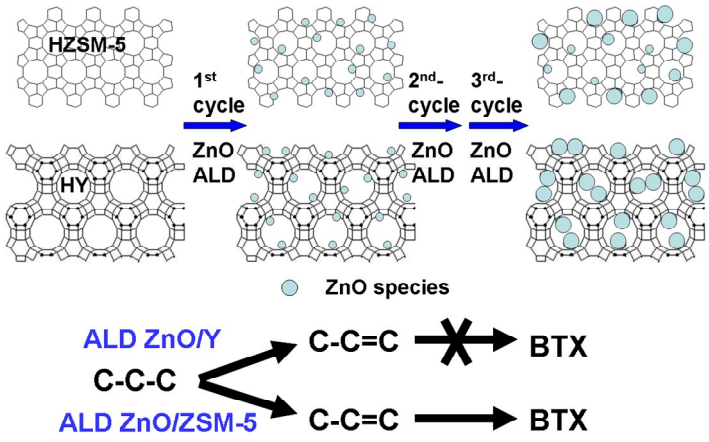

Zeolites supported highly dispersed ZnO fabricated by ALD are effective catalysts for conversion of propane to propylene and aromatics.

Introduction

Zeolites are being extensively used as acid catalysts in petroleum refining and petrochemical industries.[1, 2] Due to their large surface area, excellent reactivity and stability, unique pore structure and shape selectivity, zeolites are employed in a wide spectrum of reactions including cracking, dehydrogenation, isomerization, oligomerization, and aromatization.[3] Modification of zeolites with metal cations is an effective method of improving the catalytic performance by means of adjusting the acid properties and introducing different active species.[4] Particularly, zinc modified zeolites are effective catalysts for dehydrogenation and aromatization of light alkanes.[5-15] Zn-containing zeolites are usually synthesized by traditional techniques such as ion exchange (IE) or incipient wetness impregnation (IWI). These wet chemistry based techniques will lead to incorporation of various Zn species to the zeolite, inlcuding isolated Zn^{2+} or $Zn(OH)^{+}$ cations localized at the exchange positions, binuclear $(Zn\text{-}O\text{-}Zn)^{2+}$ or multinuclear $(Zn\text{-}(O\text{-}Zn)_n)^{2+}$ clusters, as well as bulk ZnO resulting from over-exchanges.[13, 14] In the IE process, the cation population that can be introduced into the zeolite is usually limited by the requirement of cation charge balance. Higher metal loading capacity can be achieved with the IWI method; however, higher Zn loading by IWI will inevitably lead to un-controlled aggregation of ZnO and blocking of the zeolite pores. Besides these aqueous solution based methods, chemical vapor deposition (CVD) has also been employed to introduce Zn species into zeolites. Zn^{2+} ions have been incorporated into HZSM-5 by chemical reaction between zinc vapor and Brønsted acid sites (BAS) of the zeolite at high temperatures.[16-19] Alternatively, CVD was carried out with dimethyl zinc (DMZ) at room temperature and proceeded stochiometrically with respect to the number of BAS on HZSM-5; the remaining methyl groups could be removed by higher temperature reduction with hydrogen or oxidation with oxygen, leading to Zn^{2+} ion or $Zn_nO_m^{n+}$ clusters.[13] It was discovered that highly dispersed oxygenated zinc complexes exhibit higher activities towards propane activation than isolated Zn^{2+} sites and more agglomerated forms of ZnO. However, CVD is a nonself-limiting process in which a continuous precursor stream is performed.[20] Therefore, the CVD method is lack of precise control over the dispersion and form of active species.

Originally based on CVD, in recent years atomic layer deposition (ALD) has emerged as an effective technology to synthesize catalytic materials at atomic scale precision.[21-25] In an ALD process, two gaseous precursors are pulsed alternatively such that each reacts with the surface functional groups generated during the previous pulse to produce a deposition cycle.[26] This unique deposition pattern effectively avoids channel blocking in porous systems and ensures excellent film uniformity on almost any substrate.[27-34] A large number of high surface area materials, including silica gel, zeolites, and various forms of carbon materials, have been used as substrates for ALD catalyst fabrication.[27-29] For example, Sree et al. fabricated ultra stable Y (USY) zeolite with ALD Al_2O_3, the modification led to enhanced acidity and

catalytic activity of the USY zeolite.[31] Vuori et al. supported iridium on H-beta zeolite by ALD, producing an active catalyst for ring opening of decalin.[33] In terms of alkane conversion, Feng et al. deposited vanadium oxides onto the internal walls of anodic aluminum oxide (AAO) by ALD and turned this nanoporous structure into a novel catalytic system named the catalytic nanolith.[35] For the oxidative dehydrogenation (ODH) of cyclohexane, the nanolith catalytic system was superior to a conventional powdered catalyst in terms of both efficiency and in reducing the over oxidation. By varying the number of ALD cycle, the structures of VOx sites could be precisely tuned. In the ODH reaction, polyvanadate sites were shown to be more active than monovanadate sites. However, numerical modeling of the reaction pathways indicated that the olefin formation rate was ~3 times faster on monomeric VOx sites than on polymeric VOx.[25]

Both DMZ and diethyl zinc (DEZ) have been used as precursors for ZnO ALD. The latter reagent is more frequently used because it has an adequate vapor pressure and is easier to handle and safer to use. The binary reaction of ZnO ALD using DEZ and water as the precursors is presented as below:

$$||\text{-}OH^{*} + C_2H_5ZnC_2H_5 \rightarrow ||\text{-}OZnC_2H_5^{*} + C_2H_6 \quad (1)$$

$$||\text{-}OZnC_2H_5^{*} + H_2O \rightarrow ||\text{-}OZnOH^{*} + C_2H_6 \quad (2)$$

In above equations the symbol "||-" represents the substrate and "*" denotes the surface species involved in the ALD reaction. The first half reaction of ZnO ALD on zeolites will proceeds in a similar manner as the CVD with DMZ. Instead of higher temperature reduction or oxidation, water vapor is introduced to convert surface ethyl groups into hydroxyl groups during the second half reaction of ZnO ALD, which also generates reaction sites for the next cycle of deposition. In principle, the ZnO cluster size can be precisely tailored by adjusting the number of ALD cycle.

In this work we take the advantage of ALD to produce highly dispersed ZnO species on ZSM-5 and Y zeolites. The physical and chemical properties of ALD ZnO modified zeolites are studied by techniques such as mass gain analysis, physical adsorption, scanning electron microscopy (SEM), X-ray diffraction (XRD), X-ray photoelectron spectroscopy (XPS), temperature programmed reduction (TPR), pyridine adsorption Fourier-transform infrared spectroscopy (Py-IR) and thermogravimetric analysis (TGA). Their catalytic performances are evaluated in propane dehydrogenation/aromatization. The relationships between the structural and chemical properties of the active phases and the catalytic performances are analyzed. Results from this work will demonstrate the unique benefits of ALD for catalyst preparation and improve understandings on alkane conversion processes over Zn-modified zeolites.

Experimental

Catalyst Preparation by ALD

The HZSM-5 (SiO_2/Al_2O_3 = 25) and HY (SiO_2/Al_2O_3 = 5.3) zeolites were supplied by the catalyst plant of Nankai University, China. ALD reactions were carried out with a homemade system based on the design of Elam and George.[36] Detailed descriptions

on this ALD system were reported elsewhere.[37-39] Prior to the ALD reaction, the samples were kept in the ALD reactor at 200℃ and 0.1 Torr for 5 hours to remove the adsorbed moisture. After drying, nearly 0.2g of the sample was weighed and held in a shallow copper container covered by a piece of stainless steel mesh. The container was inserted to the middle of the reaction chamber. The ALD reaction was carried out at 120℃ and 1.0 Torr with ultra pure nitrogen (99.999%, Xi'an Weiguang Gas Co., China) continuously purged through the reactor at a flow rate of 110sccm. ALD of ZnO was performed by alternately dose DEZ (99%, Dalian Credit Electronic Gas Co., China) and deionized water to the zeolite sample. The vapor pressures of DEZ and water were controlled at ~0.1Torr by adjusting the regulating valve of each precursor channel. The exposures of the two precursors were separated by N_2 purges. Each ALD cycle includes four consecutive steps: DEZ exposure, N_2 purge, H_2O exposure, and N_2 purge again. This sequence is named ALD pulse sequence and is usually expressed as t_1-t_2-t_3-t_4 where t_x (x=1, 2, 3, 4) represents the duration of each step. The pulse sequences used for modifications of the HZSM-5 and HY zeolites were 60-60-60-60s and 100-100-100-100s respectively. The number of ALD cycle was varied (mostly from 1 to 3) to regulate the loading and structure of ZnO supported on the zeolites. After the ALD experiments the catalysts were removed from the ALD reactor and were kept in an exsiccator. The masses of the samples were measured after they were cooled down to the room temperature. The zeolites fabricated by ZnO ALD were denoted as x-c-ZnO-ZSM-5 or x-c-ZnO-Y, where x represents the number of ALD cycle.

Characterization

The surface areas and pore volumes of the catalyst samples were determined by N_2 physisorption technique using a Micromeritics ASAP 2010 instrument. The samples were degassed at 250℃ for 10h prior to adsorption experiments. The accurate content of Zn in each zeolite sample was analyzed by a Perkin Elmer 7000DV inductively coupled plasma atomic emission spectrometer (ICP-AES). XRD characterizations were conducted on a Rigaku D/Max 2400 spectrometer using Cu Kα radiation. Surface morphologies of the catalyst samples and distributions of the Zn element were characterized by a FEI Quanta 600 FESEM equipped with an energy dispersive X-ray spectrometer (EDX). XPS spectra of the catalyst samples were taken with a Thermo Scientific K-Alpha instrument using Al Kα radiation source (1468.68 eV). The XPS peaks were calibrated by the binding energy of C_{1s} peak at 284.6 eV.

TPR measurements were carried out with a Micromeritics AutoChem 2950 HP automated catalyst characterization system. The samples were pretreated at 300℃ in a N_2 stream and then cooled down to 50℃. Reduction was carried out in a flow of H_2/Ar (10 vol%) from 50 to 800℃ with a heating rate of 20℃/min. The H_2 consumption was measured by the TCD.

Py-IR characterizations were performed with a VERTEX 70v FTIR spectrometer. The catalyst samples were pressed into self-supporting disks. The sample cell was evacuated at 400℃ for 2 h; the background spectrum was measured after the sample cell was cooled to room temperature. Pyridine vapor was introduced into the sample cell for 0.5hr at room temperature. FTIR spectra were taken after the sample cell was

evacuated at elevated temperatures.

Thermogravimetric analyses (TGA) of the used catalysts were performed with a TA TGA/DTA instrument. During the measurements the temperature was varied from 50 to 900℃ with a heating rate of 10℃/min under air flow.

Catalytic performance evaluation

Catalysis tests were carried out in a 4 mm i.d. fixed-bed micro-reactor made of quartz. 50-70mg of catalyst was used in each test. The exact amount of the catalyst charged to the reactor was adjusted based on the ZnO loading to make sure a same amount of zeolite (~45mg) was used. The reactant was 5 vol% C_3H_8 mixed with Ar and was pushed through the reactor at a rate of 10sccm (with a WHSV of 400 h^{-1}). The reactions were carried out in the temperature range of 400-600℃ at ambient pressure. The reaction products were analyzed online by an Agilent 7820 GC equipped with a TCD and an FID detector. A PLOT-Al_2O_3/KCl column (50m×0.53mm×15um) was used to separate light organic products. Aromatic products were separated by an HP-5 column (30m×0.320mm×0.25um).

Results and Discussion

The parent HY and HZSM-5 zeolites have fairly large surface areas. The large surface area and the sub-nanometer pore structure may require a long time for the ALD reaction to complete. To explore the saturation conditions of ZnO ALD on the zeolites, a series of experiments with pulse sequences of x – x – x – x seconds were carried out, in which x was varied from 5 to 100s. Figure 1a presents the mass gains on the two types of zeolites with different precursor dosing times after 1-cycle ZnO ALD. For both zeolites the mass gain curves level off at large precursor exposures, which is an indication of the self-limiting surface reaction typical for ALD processes. On HZSM-5 saturation of the ALD surface reaction is almost achieved with a precursor exposure of 30s; a longer precursor exposure of 50s is required for saturated surface reaction on HY. Based on these results, the pulse sequence used for fabrication of ZSM-5 is 60-60-60-60s and a pulse sequence of 100-100-100-100s is applied for fabrication of Y zeolite.

Figure 1b displays the sample mass gain data versus the number of ALD cycle obtained on HZSM-5 and HY under saturated ALD reaction conditions. The distinct shapes of the mass gain curves probably reflect the different pore structures of the two types of zeolites. The 10-member-ring structure of ZSM-5 has a pore size of 0.53-0.56nm; while the average diameter of the 12-member-ring channel of Y zeolite is 0.74nm.[31, 40, 41] The linear DEZ molecule has a diameter of 0.53nm.[42] Since the micropore size of HZSM-5 is slightly larger than the diameter of DEZ, the DEZ molecules should be able to enter the micropores of HZSM-5 and react with the hydroxyl groups on the internal surface. Each ALD reaction has a reactive sticking coefficient, which refers to the ratio of the collisions that result in a surface reaction to the total number of collisions between the precursor and the substrate. The most efficient ALD processes (such as the ALD reactions using metal alkyls and water as the precursors) have reactive sticking coefficients on the order of 10^{-4}–10^{-3}.[36] This means the DEZ molecules diffused into the pores during the first ALD cycle should

have plenty of chances to react with the hydroxyls located deeper inside the microchannels rather than only react with the hydroxyl groups near the pore openings. After the first ALD cycle the pores on ZSM-5 may be reduced to a degree that it becomes much harder for DEZ to penetrate. Therefore it is very likely that on ZSM-5 the 2nd and subsequent cycles of ALD reaction mostly occur on the external surface. From Figure 1b it can be noticed that ~9% of mass increase is obtained on HZSM-5 after the first cycle of ZnO ALD and the mass gain increases to ~16% or ~22% as the number of ALD cycle is further increased to 3 or 8. The smaller and smaller increase in sample mass with the increasing number of ALD cycle is an indication of the gradually reduced available surface for ALD.

Compared to HZSM-5 the sample mass gain due to ALD of ZnO is much larger on HY. The sample mass increases steeply for the first 3 cycles of ALD and a ~40% mass gain is achieved with 3 cycles of ZnO ALD. Because the micropore size of HY is much larger than the diameter of DEZ, during the first 3 cycles of ZnO ALD although the pore size is gradually reduced after each ALD cycle, the remaining clearances are sufficient for DEZ molecules to diffuse through so that the internal surfaces are still available for the ALD reaction. This stage corresponds to the initial linear mass increase on Y zeolite with the increasing number of ALD cycle. After the 3rd ALD cycle, the micropores on Y zeolite become severely blocked. DEZ molecules can no longer enter the microchannels and the ALD reaction can only occur on the external surface. With the increasing number of ALD cycle the further increase in sample mass will become much slower, similar to the situation on ALD ZnO modified ZSM-5. In the mean time, with more than 3 cycles of ZnO ALD coating the moisture absorption ability of the Y zeolite is affected. The abatement of moisture absorption is more serious with more cycles of ALD coating. This means that upon exposure to air the ALD ZnO fabricated Y zeolite will absorb less moisture compared to the parent zeolite, which will lead to underestimated values of sample mass gain. As a consequence, the sample mass gain appears to stop for the Y zeolite fabricated by more than 3 cycles of ZnO ALD.

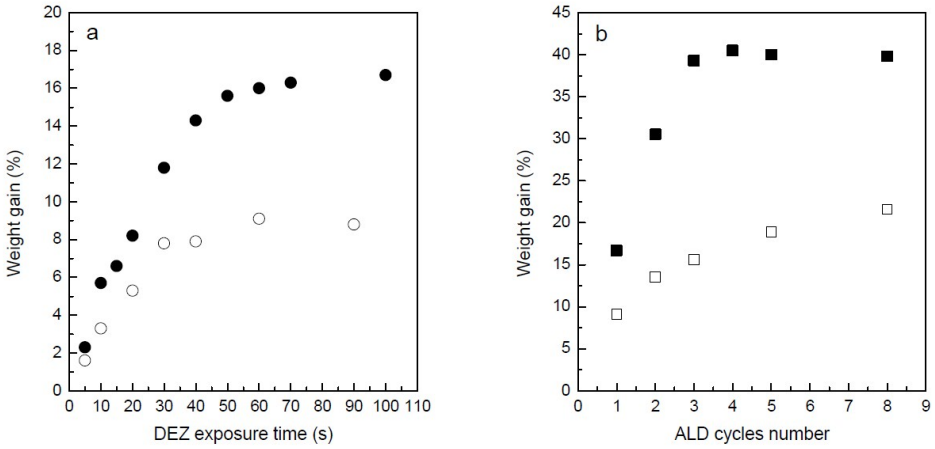

Figure 1. Saturation curves of ZnO ALD performed on HZSM-5 (open circles) and on HY (solid circles) zeolites (a). Weight gain versus the number of ZnO ALD cycle obtained on HZSM-5 (open squares) and on HY (solid squares) zeolites (b).

Table 1 Elemental analysis and textural properties of ALD ZnO modified zeolites

Sample	Zn content (wt%, ICP)	Zn content (wt%, mass gain analysis)	S_{BET} (m^2/g)	S_{micro} (m^2/g)
HZSM-5	--	--	320	159
1c-ZnO-ZSM-5	5.8	6.6	196	160
2c-ZnO-ZSM-5	6.9	9.2	200	153
3c-ZnO-ZSM-5	9.0	11.1	73	56
HY	--	--	532	405
1c-ZnO-Y	11.9	11.6	369	269
2c-ZnO-Y	20.1	19.0	307	228
3c-ZnO-Y	28.4	24.5	195	136

The elemental analysis and textural properties of ALD ZnO modified zeolites are summarized in Table 1. Comparing the wt% of Zn calculated from the sample mass gain data (assuming all forms of zinc oxides have a same chemical formula of ZnO) with those measured by ICP, the contents of incorporated Zn species measured by these two methods are generally consistent. Even with only one cycle of ALD, the loading of Zn introduced by ALD is much higher than the loading that could possibly be achieved by IE. After the modifications by ALD of ZnO, the surface areas of both zeolites are significantly reduced. Apparently, the decreased surface area is resulted from filling of the pores by ZnO species. It is worth noting that the micropore area accounts for over 3/4 of the total surface area of HY, which means that most of the reaction sites are located at the internal surface of the Y zeolite. After 3 cycles of ZnO ALD, nearly 80% of the loss surface area is micropore area, confirming that the ALD reactions mainly occur in the internal channels of the Y zeolite. For HZSM-5 the micropore area only accounts for less than 1/2 of the total surface area. Therefore a fairly large fraction of ZnO should be deposited on the external surface. Besides, due to the limited micropore size of ZSM-5, infiltration into the internal surface would become more difficult with the increasing number of ALD cycle. After 3 cycles of ZnO ALD, the total surface area of the modified ZSM-5 is reduced from 320 to $73 m^2/g$ while the micropore area decreases from 159 to $56 m^2/g$. Only 42% of the lost surface area is micropore area, indicating that a substantial portion of ZnO is deposited on the external surface when ZSM-5 is modified by multiple cycles of ALD.

X-ray diffraction measurements were carried out to determine the phase compositions of ALD ZnO modified zeolites. XRD patterns of the parent and the ALD ZnO fabricated HZSM-5 and HY are shown in Figure 2a and 2b. Generally the diffraction patterns of the original and the modified zeolites are quite similar. On both zeolites the positions of the diffraction peaks corresponding to the MFI or FAU zeolitic frameworks are almost identical before and after ZnO ALD, indicating that the ALD

reaction does not change the crystal structures of the zeolites. On both zeolites the intensities of the peaks at low diffraction angles (2θ=5-15°) are reduced. It has been demonstrated that the reduced peak intensity at low diffraction angles is attributed to foreign species (in this case, ZnO) incorporated inside the channels of the zeolites rather than collapse of the zeolitic framework.[43-46] On all ALD ZnO modified ZSM-5 samples and 1c-ZnO-Y no diffraction peaks corresponding to crystalline ZnO can be identified, implying that in these samples the deposited ZnO is in an amorphous form or big crystals of ZnO do not exist. However, on the 2-cycle and 3-cycle ALD ZnO modified Y zeolite, small peaks corresponding to [101] and [110] crystal planes of ZnO can be observed at 2θ=36.2 and 56.5º. According to the scheme of the ZnO ALD reaction described in equations (1) and (2), isolated $Zn(OH)^+$ species are produced during the first cycle of ZnO ALD; with the increasing number of ALD cycle the oxide clusters will gradually grow larger however the ZnO domain size should not reach nanometer scale by performing only a few cycles of ALD. These ZnO crystals are probably generated through dehydration between adjacent -ZnOH sites. Because multiple –ZnOH sites must be involved in the formation of ZnO crystals, the development of these ZnO nanocrystals requires a high density of –ZnOH sites. Since the attachment of Zn species relies on the chemical reaction between DEZ and the BAS, the density of –ZnOH species is determined by the concentration of the BAS. The concentration of the BAS on the HY zeolite (with a SiO_2/Al_2O_3 ratio of 5.3) is much higher than that on the HZSM-5 zeolite (with a SiO_2/Al_2O_3 ratio of 25). Therefore formation of ZnO crystals is much easier on ALD ZnO modified Y zeolite. Based on the Debye-Scherrer equation, the average sizes of the ZnO crystals are estimated to be 7~10 nm. Due to the very limited size of the micropores, these ZnO nanocrystals must be formed on the external surface of the Y zeolite. Since most of the ZnO is believed to be deposited inside the microchannels, these nanocrystals should not represent majority of the ZnO species deposited on the Y zeolite.

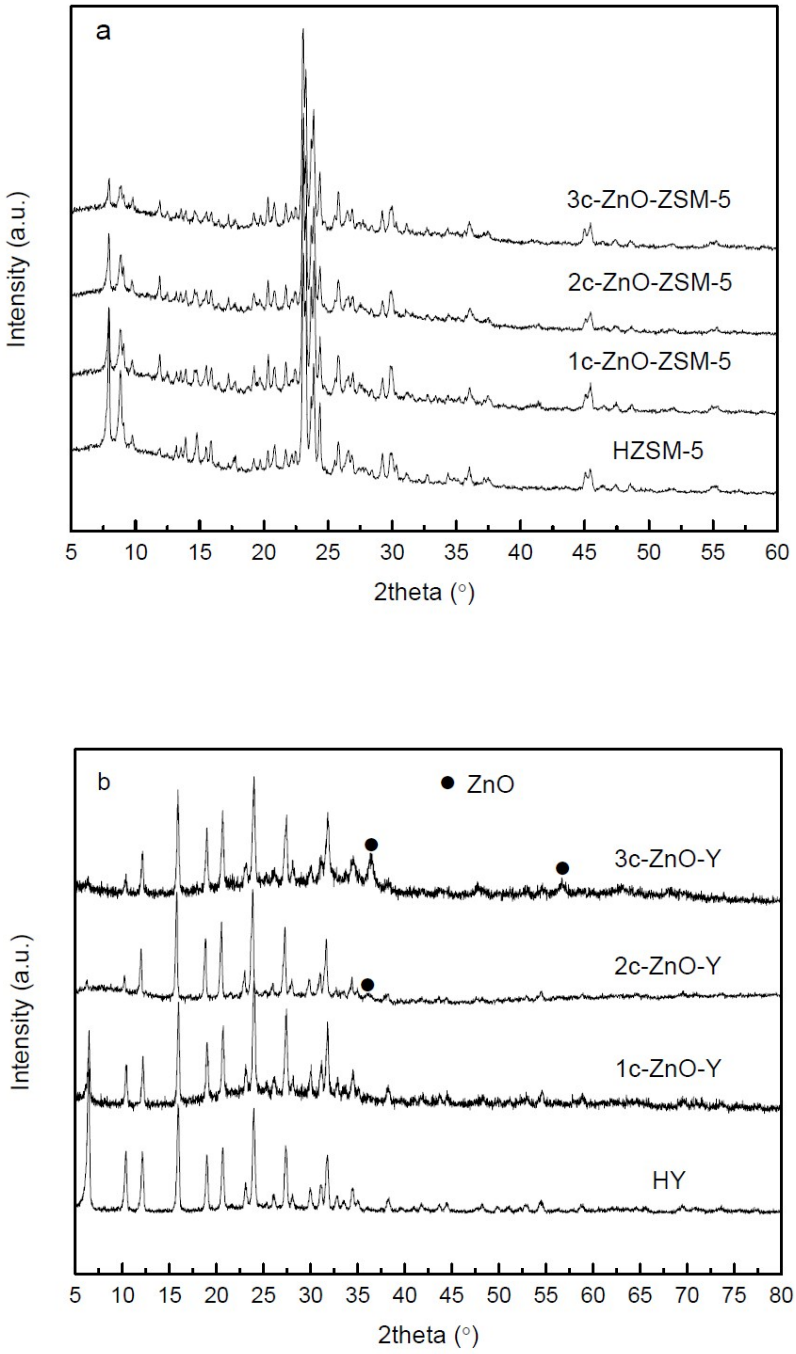

Figure 2. XRD patterns of ALD ZnO modified ZSM-5 and Y zeolites

Structures and morphologies of the ALD ZnO modified zeolites are studied by SEM. Figure 3 displays representative SEM images of the ALD ZnO modified ZSM-5 and Y zeolites. Generally, the shapes and morphologies of the ALD ZnO fabricated zeolites are very similar to those of the parent zeolites. Large aggregates of ZnO

domians can not be observed, indicating uniform distribution of ZnO species on the supports. For 1 to 3 cycles of ZnO ALD modified ZSM-5 and 1-cycle ZnO ALD modified Y zeolite, the surfaces of the zeolite crystals are quite smooth (Figure 3a-d) and no feature from the oxide films can be observed. However, tiny grains of nanoparticles can be observed on the surface of Y zeolite fabricated by performing 2 or 3 cycles of ZnO ALD (Figure 3e, 3f). These ZnO nanoparticles are uniformly distributed on the surfaces of zeolite crystals and their average size is around 10nm. The size of ZnO nanocrystals found in the SEM images agrees with the results derived from XRD patterns using the Debye-Scherrer equation. EDX mapping analyses were performed on selected catalyst samples (3c-ZnO-ZSM-5 and 3c-ZnO-Y). The signal patterns of Si, O, and Zn overlap perfectly, confirming complete and conformal coating of the zeolites by ALD ZnO (data not shown).

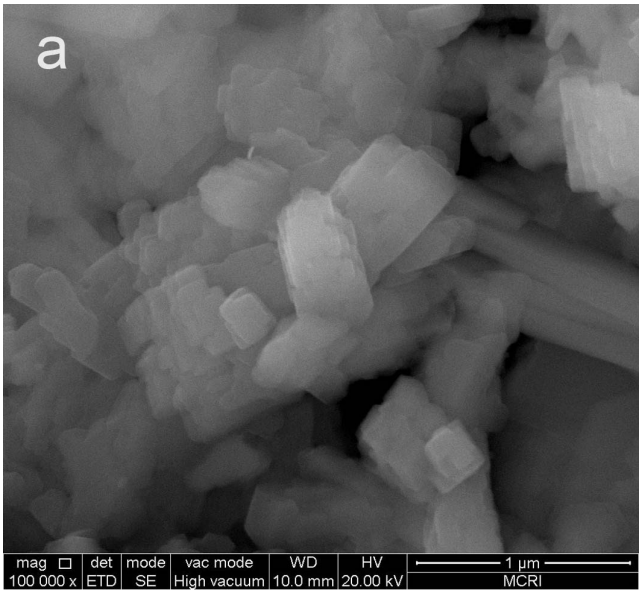

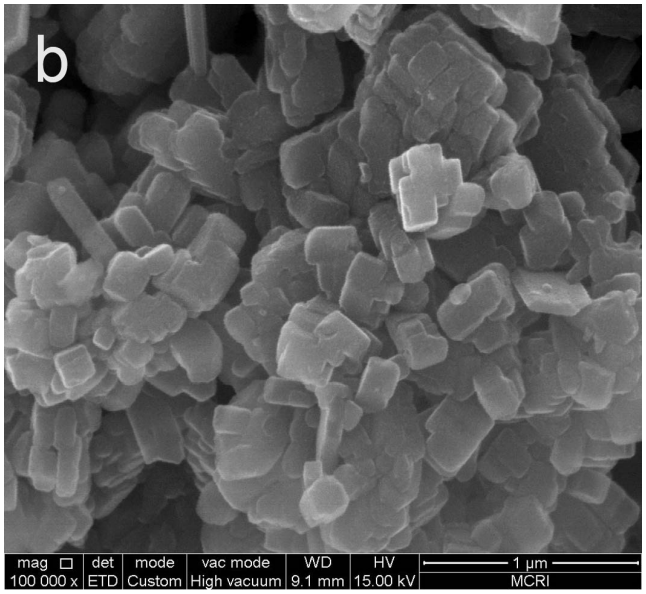

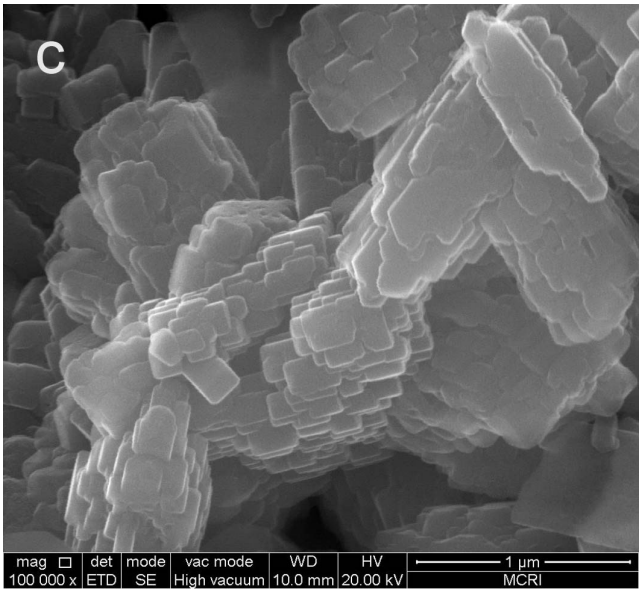

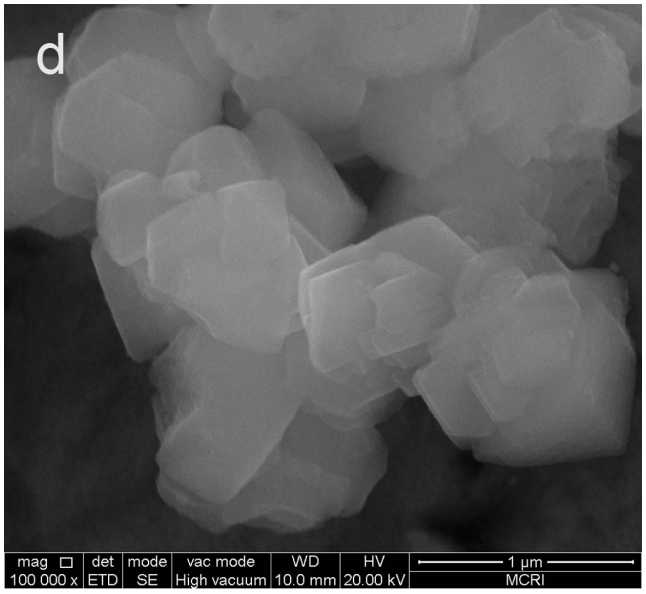

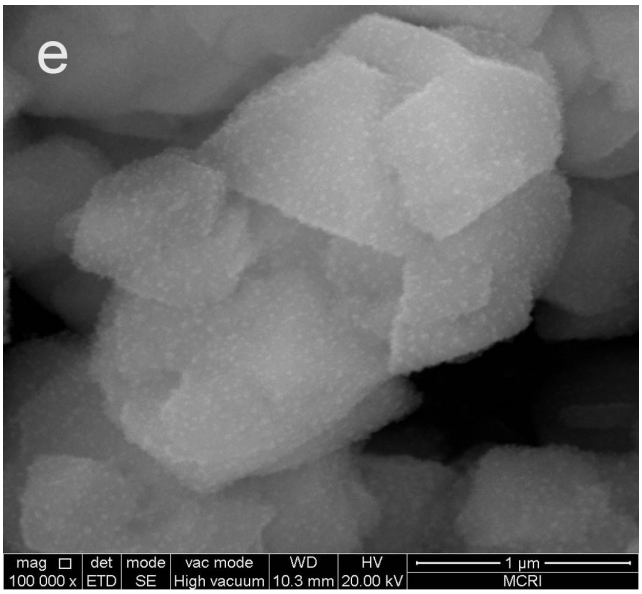

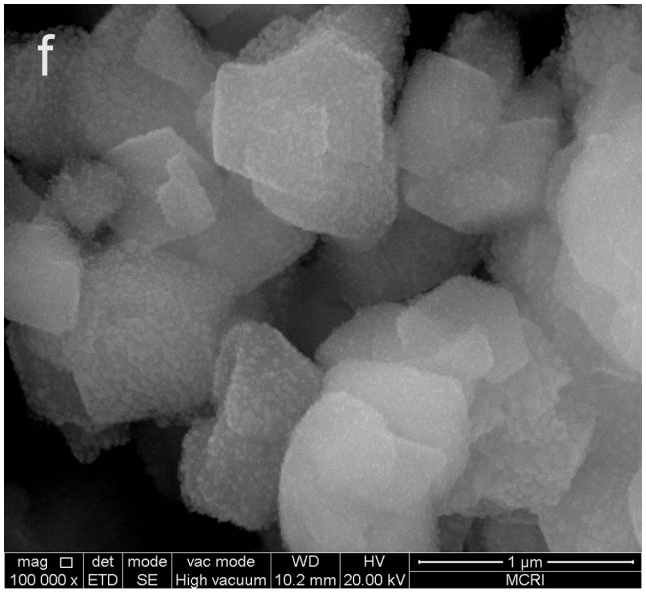

Figure 3. SEM images of ALD ZnO modified ZSM-5 and Y zeolites: (a) 1c-ZnO-ZSM-5, (b) 2c-ZnO-ZSM-5, (c) 3c-ZnO-ZSM-5, (d) 1c-ZnO-Y, (e) 2c-ZnO-Y, (f) 3c-ZnO-Y.

XPS characterizations were carried out to give insights into the electronic states of the Zn species deposited on the zeolites. The XPS spectra of the Zn($2P_{3/2}$) region of a pure ZnO reference sample and the ALD ZnO modified ZSM-5 and Y zeolites are displayed in Figure 4. The Zn^{2+} species in the ZnO nano powder has a binding energy (BE) of 1020.77 eV. The BE of the Zn species in the ALD ZnO modified ZSM-5 and Y zeolites are considerably higher than that of the pure ZnO. The peak of Zn($2P_{3/2}$) has the highest BE when the zeolite is fabricated by only 1 cycle of ZnO ALD (1022.40 eV for 1c-ZnO-ZSM-5 and 1022.70 eV for 1c-ZnO-Y); and it gradually shifts to lower BE with the increasing number of ALD cycle. In previous studies a high BE peak at around 1023.0 eV was assigned to isolated $Zn(OH)^+$ due to the stronger interaction between Zinc and protonic acid sites.[9] Moreover, Tamiyakul, et al. confirmed that the Zn species localized at the cation exchanged sites has a high BE of about 1023.2 eV because the lattice oxygen of the zeolite exhibited higher electronegativity than the O^{2-} ligand in bulk ZnO.[12] Based on the scheme of the ALD reaction, isolated $Zn(OH)^+$ species are anchored to the support through the lattice oxygen of the zeolite during the first cycle of ZnO ALD; in subsequent ALD cycles Zn species are grafted through the hydroxyl groups formed in the previous deposition cycle. As a consequence highest positive shifts of the BE should be observed on the zeolites fabricated by only 1 cycle of ZnO ALD. With the increasing number of ALD cycle, the average size of ZnO clusters progressively grows larger and their structures gradually change towards that of bulk ZnO; accordingly the BE of the Zn species gradually approaches that of the pure ZnO reference sample.

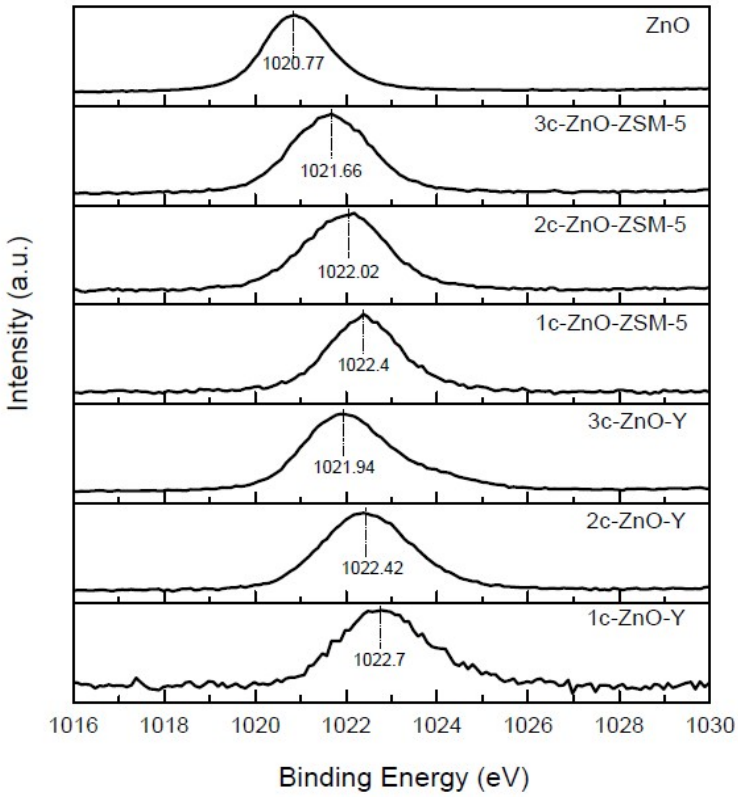

Figure 4. XPS spectra of ALD ZnO modified ZSM-5 and Y zeolites

TPR profiles of the ZnO nano powder reference sample and the ALD ZnO modified ZSM-5 and Y zeolites are presented in Figure 5. Two sets of reduction peaks can be observed for the ZnO reference sample: a small fraction of the sample is reduced around 518℃ and majority of the sample is reduced at temperatures higher than 700℃. The reduction temperature of ZnO has been a topic of discussion in the literature. It seems that the size and structure of ZnO domains have great impact on the reduction temperature. Fu et al. found that very small ZnO particles can be reduced at a relatively low temperature (386℃), whereas large particles are reduced at a higher temperature (675℃).[11] Biscardi and Popov et al. discovered that bulk ZnO shows a broad reduction band above 600℃.[7, 47] Liao et al. observed two reduction peaks (600 and 750℃) on plate-shaped ZnO, while only one reduction peak was obtained on long rod-shaped nanoZnO at 600℃.[48] Based on these findings, it is proposed that poorly crystallized ZnO can be reduced at lower temperatures and large crystals of ZnO suppress their reducibility.[11, 49] From the TPR profile shown in figure 5, it can be inferred that both forms of ZnO co-exist in the nanoZnO reference sample. The 1c-ZnO-ZSM-5 shows only one reduction feature at 520℃, which is close to the low-temperature reduction peak of nanoZnO. Because isolated $Zn(OH)^+$ is the predominant form of ZnO on 1c-ZnO-ZSM-5, this low-temperature reduction peak should correspond to reduction of the isolated $Zn(OH)^+$ species. With the increasing number of ALD cycle, the portion of ZnO that is reduced at the higher temperature

range (780-800℃) gradually increases. These high temperature bands should represent reduction of larger Zn_mO_n clusters whose structures are close to bulk ZnO. It is worth noting that for all ALD ZnO modified ZSM-5 samples the positions and intensities of the low-temperature reduction peaks are comparable, implying that isolated $Zn(OH)^+$ species always exists despite the increment in the number of ALD cycle. As mentioned earlier, the pore size of HZSM-5 is very close to the diameter of DEZ. Consequently the precursor molecules could infiltrate the micropores almost only during the first cycle of ALD fabrication. During subsequent ALD cycles most of the isolated $Zn(OH)^+$ species distributed in the internal cavities of ZSM-5 probably remains unchanged while bulky Zn_mO_n clusters are gradually formed on the external surface.

The TPR profiles of ALD ZnO modified Y zeolites share some common features with those of ALD ZnO modified ZSM-5. The low-temperature and high-temperature reduction peaks observed on these samples demonstrate the existence of the isolated (amorphous) $Zn(OH)^+$ and more crystallized Zn_mO_n clusters/particles respectively. Compared to ALD ZnO modified ZSM-5, the lower temperature reduction peak shifts from 520-540℃ to 560-570℃. Besides, both the low-tempeature and high-temperature reduction peaks can be observed on the Y zeolite fabricated by only 1 cycle of ZnO ALD. These evidences suggest that the average size of ZnO domains is larger on ALD ZnO modified Y zeolites. As discussed before, growth of the ZnO domain is probably resulted from dehydration between adjacent –ZnOH species and this behavior is closely related to the density of surface -ZnOH sites or the loading of ZnO. With the increasing number of ALD cycle, the intensity of the low-temperature reduction peak decreases and that of the high-temperature peak increases, indicating that isolated or amorphous $Zn(OH)^+$ species are gradually transformed into more bulky Zn_mO_n clusters. For 3c-ZnO-Y, the peak at the lower temperature almost diminishes and a large reduction peak is observed at ~772℃, indicating that nearly all isolated $Zn(OH)^+$ species have transformed into Zn_mO_n clusters or particles. The micropore size of Y zeolite is much larger than the diameter of DEZ so that the precursor molecules could easily enter the micropores during the first three cycles of ZnO ALD. Consequently on both internal and external surfaces of Y zeolite the isolated $Zn(OH)^+$ species produced in the first ALD cycle could be converted to Zn_mO_n clusters or particles in the following ALD cycles.

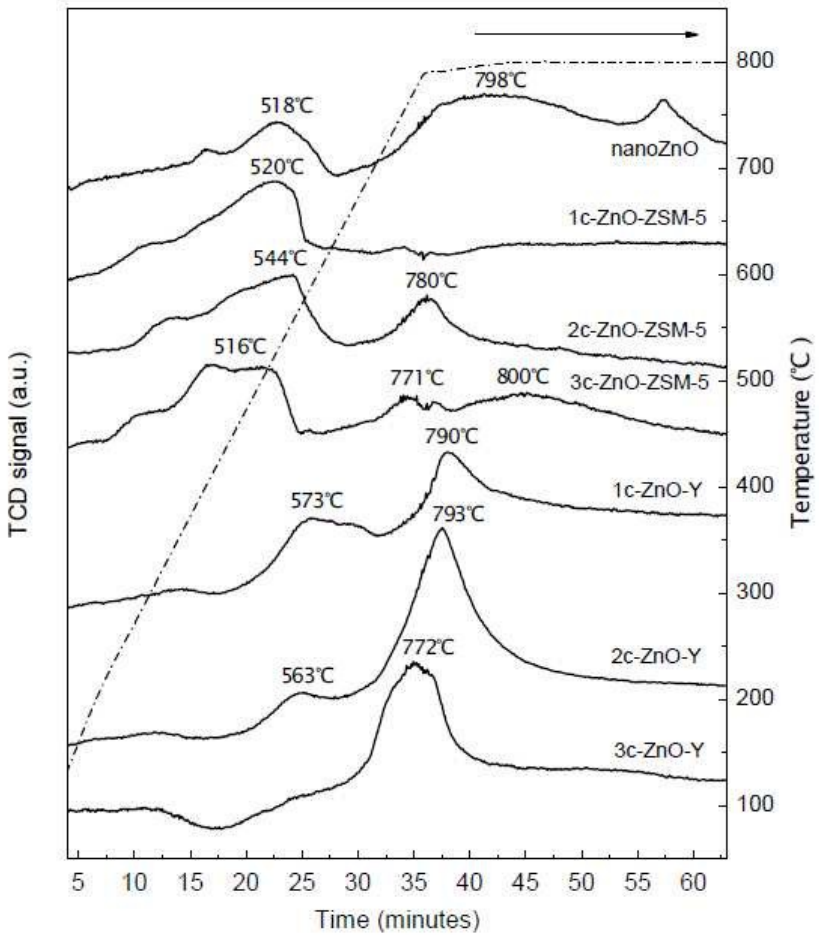

Figure 5. TPR profiles of ALD ZnO modified zeolites and the nanoZnO reference sample

The acid properties of the ALD ZnO modified zeolite samples were characterized by FTIR spectroscopy of adsorbed pyridine. The FTIR spectra of pyridine adsorbed on the ALD ZnO modified zeolite samples are shown in Figure 6. The IR band at 1540~1550cm^{-1} corresponds to pyridine adsorbed on Brønsted acid sites (BAS) and the band at 1450~1455cm^{-1} presents pyridine adsorbed on Lewis acid sites (LAS). Acid sites that adsorb pyridine molecules at 150℃ are considered total acid sites and strong acid sites can retain pyridine at temperatures as high as 350℃.

On 1c-ZnO-Y the adsorption band at ~1540cm^{-1} completely disappears after evacuation at 150℃, indicating that the BAS are completely eliminated by ALD of ZnO. This result is consistent with the scheme of ZnO ALD reaction in which DEZ molecules are anchored to the zeolite through stoichiometric reaction with the acidic surface protons (BAS). At the same time, the adsorption band at ~1450cm^{-1} increases dramatically, indicating a significant enhancement in the number of LAS, which is apparently due to the Lewis acidity of incorporated ZnO. After desorption at 350℃, nearly 90% of the adsorbed pyridine is retained, which suggests that the acidity of

these LAS is quite strong. As the number of ZnO ALD cycle is increased from 1 to 3, no much change to the IR spectra can be observed. The band at ~1450 cm^{-1} becomes broader and the peak area becomes slightly smaller, implying a reduced number of LAS accessible to pyridine molecules which is probably resulted from aggregation of ZnO domains or blocking of the micropores. After evacuation at 350℃, the peak area almost remains constant, indicating that the strong acidity of these LAS. In summary, fabrication of HY by ZnO ALD eliminates the BAS and significantly enhances the number and strength of LAS.

On 1c-ZnO-ZSM-5 the pyridine adsorption band at ~1550cm^{-1} is reduced by ~80% compared to the parent HZSM-5 zeolite. This means that on ZSM-5 the BAS are only partially removed after the modification by ZnO ALD. The reason for the incomplete reaction between DEZ and the BAS probably lies in the smaller size of the micropores of ZSM-5 that impedes the accessibility of DEZ molecules to all reactive sites. After the ALD fabrication the peak at ~1455cm^{-1} becomes much more noticeable, which is an indication of the greatly increased number of LAS from the deposited ZnO. After desorption at 350℃, the pyridine adsorption peak at ~1455cm^{-1} remains almost unchanged while the band at ~1545cm^{-1} is reduced by ~45%. These results suggest that the acidity of the LAS from the incorporated ZnO is fairly strong while part of the remaining BAS on ZSM-5 have weak to medium acidity. According to these Py-IR spectra, varying the number of ALD cycle does not cause too much change to acid properties of the ALD ZnO modified ZSM-5.

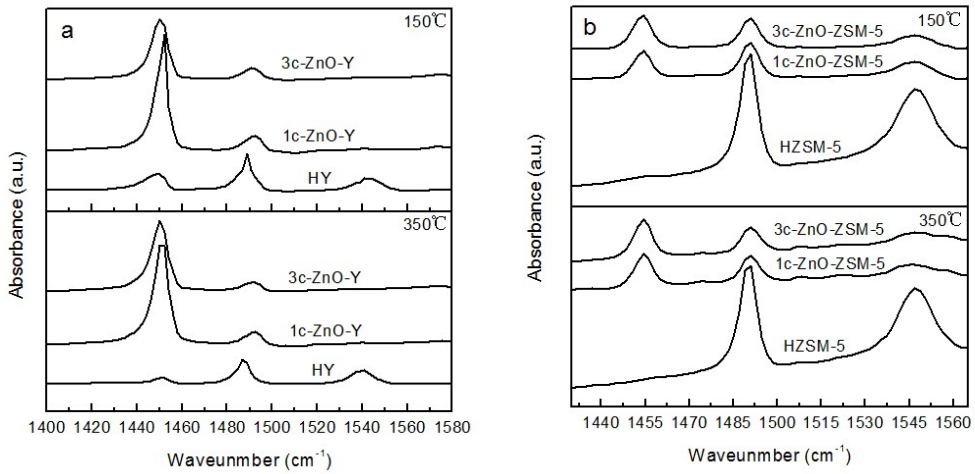

Figure 6. IR spectra of pyridine adsorbed on the parent HZSM-5 and on ALD ZnO modified ZSM-5 catalysts (a); and on HY and ALD ZnO modified Y zeolite (b). The upper panels represent the spectra taken after evacuation at 150℃ and the lower panels display the spectra taken after evacuation at 350℃.

Figure 7 presents the catalytic performances of the parent and ALD ZnO modified Y zeolite in propane conversion measured at a reaction time of 30min. The activity of the unmodified HY sample is quite low: less than 3% of propane is reacted at 550℃. The product distribution is 30-40% propylene and 60-70% cracking products including methane, ethane, and ethylene. No aromatics were detected from the

reaction products. Incorporation of ZnO considerably promotes the activity of the Y zeolite. The conversion at 550℃ rises to 11-16% on the zeolite fabricated by 1-3 cycles of ZnO ALD. Dehydrogenation becomes the major reaction path on these ALD ZnO modified Y zeolites. The selectivity to propylene is over 85% at temperatures ≥ 500℃. Nearly 10% of the reacted propane is converted to cracking products and less than 5% is converted to aromatics. The catalytic properties of HY are primarily from the BAS. It has been proved that all BAS are replaced by ZnO species in the ALD reactions; therefore the catalytic performances of ALD ZnO modified Y zeolites should be similar to those of ZnO. Since ZnO is an active dehydrogenation catalyst, it is reasonable to expect propylene to be the dominant reaction product on ALD ZnO modified Y zeolite.

The conversion of propane on the Y zeolite modified by different cycles of ZnO ALD increases in sequence: 1c-ZnO-Y < 3c-ZnO-Y < 2c-ZnO-Y. Because the catalytic activity of ALD ZnO modified Y zeolite mostly comes from the incorporated ZnO, the enhanced conversion with the increased number of ALD cycle is probably a reflection of the increased number of active sites which is obviously related to the higher loading of ZnO. As the number of ALD cycle is further increased to 3, aggregation of ZnO domains and blocking of the micropores become more severe, which could lead to a reduced number of available active sites. It is worth mentioning that although the 2c-ZnO-Y sample exhibits a higher propane conversion, its catalytic activity on the basis of per zinc atom is even lower than that of 1c-ZnO-Y. This suggests that the dehydrogenation activity of isolated $Zn(OH)^+$ species may be better than small clusters of ZnO.

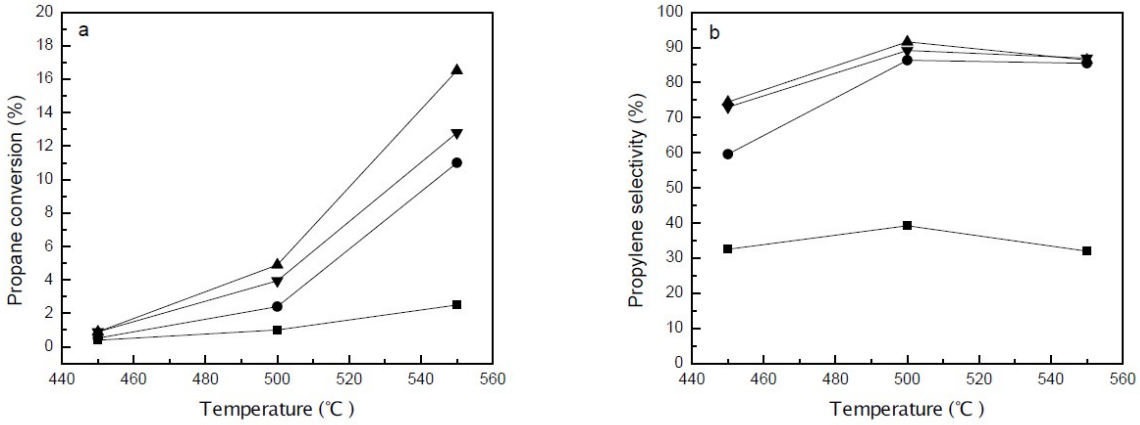

Figure 7. Conversion of propane (a) and selectivity to propylene (b) over the parent HY and ALD ZnO modified Y zeolites: (■) HY, (●) 1c-ZnO-Y, (▲) 2c-ZnO-Y, (▼) 3c-ZnO-Y (T= 450-550℃, WHSV= 400 h^{-1})

Figure 8 displays the conversion and selectivity of the parent and ALD ZnO modified ZSM-5 zeolite in propane dehydrogenation/aromatization measured at a reaction time of 30min. On un-modified HZSM-5 ~3% conversion of propane can be achieved at 500℃ and the conversion increases to ~16% at 550℃. At all tested temperatures

cracking is the dominant reaction path in that over 80% of the reacted propane is converted to C_1 and C_2 molecules (methane, ethane, and ethylene). The selectivity to propylene is 10-20% and the selectivity to aromatics is below 5%. After the modification by ALD of ZnO the catalytic activity of ZSM-5 is greatly enhanced. The propane conversion at 500℃ is over 50% and it reaches ~90% at 550℃. Dehydrogenation and aromatization become primary reaction paths. The combined selectivity to propylene and BTX is 50-60%. Nearly 40% BTX yield can be achieved at 550℃. Apparently the promoted dehydrogenation activity is from the incorporated ZnO species. As evidenced by Py-IR measurements, after the ALD fabrication all BAS on the Y zeolite are eliminated while some BAS on the ZSM-5 survived. Normally BAS are believed to be responsible for converting olefins to aromatics through reaction paths such as oligomerization and ring-closure.[18, 50, 51] Furthermore, Stepanov et al has proposed a synergetic effect of ZnO and BAS on the aromatization activity of Zn-loaded zeolites.[52-54] Therefore the remaining BAS on the ALD ZnO modified ZSM-5 are crucial for further converting propylene to BTX.

The catalytic performances of ZSM-5 modified by different cycles of ZnO ALD are generally comparable. As has been discussed for multiple times, since the pore size of ZSM-5 is very close to the diameter of DEZ, the precursor molecules could only infiltrate the micropores during the first cycle of ALD; in the following ALD cycles the most active isolated $Zn(OH)^+$ species and the BAS located inside the microchannels probably remain almost unchanged. The more bulky Zn_mO_n clusters formed on the external surface may have very little extra contribution to the catalytic activity, especially to the production of BTX because the BAS located at the external surface should have been neutralized. Based on the results of catalysis experiments, a most effective propane dehydrogenation/ aromatization catalyst should be produced by performing only one cycle of ZnO ALD to ZSM-5 zeolite.

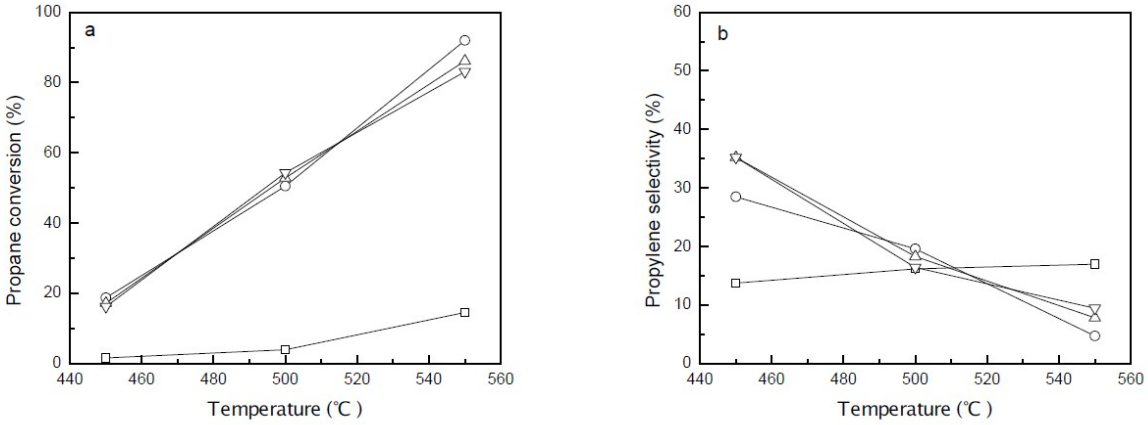

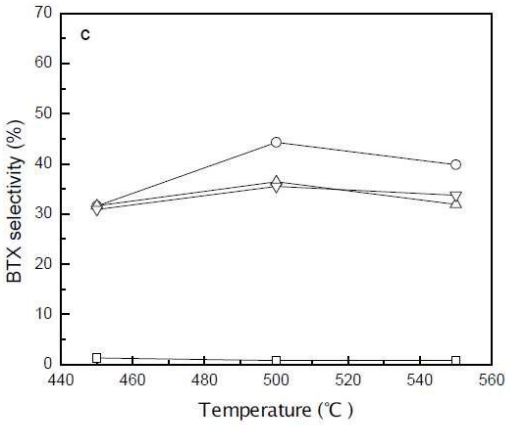

Figure 8. Conversion of propane (a) and selectivity to propylene (b) and BTX (c) over the parent HZSM-5 and ALD ZnO modified ZSM-5 zeolites: (□) HZSM-5, (○) 1c-ZnO-ZSM-5, (△) 2c-ZnO-ZSM-5, (▽) 3c-ZnO-ZSM-5 (T= 450-550℃, WHSV= 400 h^{-1})

The long-term stabilities of these ALD ZnO modified zeolites are inspected at 550℃. Figure 9 and figure 10 respectively show the catalytic performances of ALD ZnO modified Y and ZSM-5 zeolites in the stability tests. Unfortunately, although the ALD ZnO modified zeolites exhibit fairly high initial activities, their activities decrease rapidly with further extended time on stream. After 10 hrs of continuous running, the propane conversion on ALD ZnO modified Y zeolite drops to 4-6%; and only ~3% conversion is left on ALD ZnO modified ZSM-5. Coke formation is most likely the main reason for deactivation of these catalysts. After the stability tests the color of the catalyst samples changes from white to black. TGA measurements reveal that carbon-like deposits account for 13.0 wt% of the used 1c-ZnO-Y and 6.6 wt% of the used 1c-ZnO-ZSM-5. Coking has been the primary reason for catalyst deactivation in non-oxidative dehydrogenation reactions. The coke species formed during the reaction may gradually cover the active sites and block the micropores, and eventually lead to malfunctioning of the catalyst. During the stability test the product distribution almost stays constant for ALD ZnO modified Y zeolite; however for ALD ZnO modified ZSM-5 the major reaction product gradually changes from BTX to propylene along with the deactivation of the catalyst. Since the BAS are responsible for converting olefins to aromatics, gradual coverage of the BAS by coke species during deactivation of ALD ZnO modified ZSM-5 may lead to the loss of its aromatization activity.

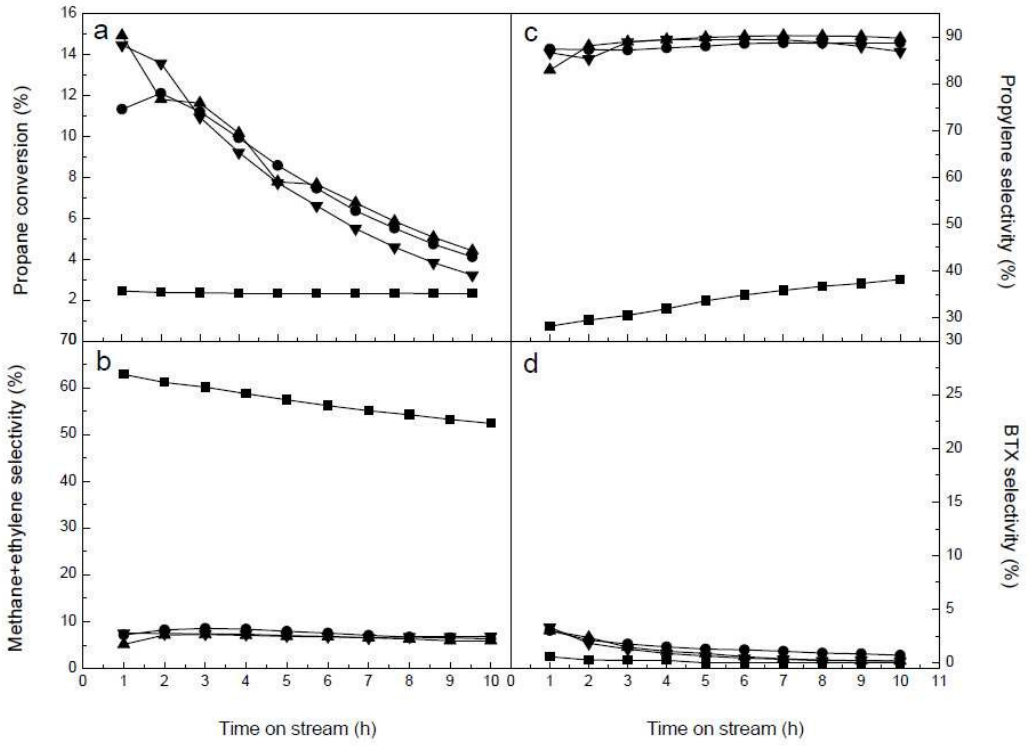

Figure 9. Conversion of propane (a) and selectivity to methane + ethylene (b), propylene (c), and BTX (d) over the parent HY and ALD ZnO modified Y zeolite: (■) HY, (●) 1c-ZnO-Y, (▲) 2c-ZnO-Y, (▼) 3c-ZnO-Y (T= 550℃, WHSV= 400 h^{-1})

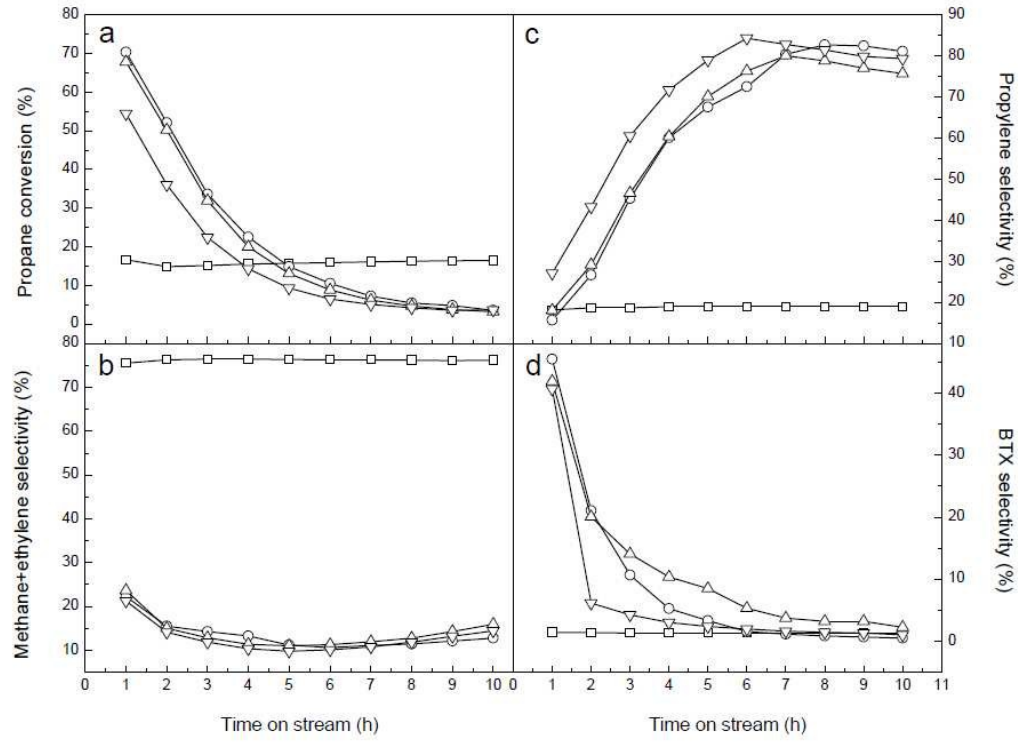

Figure 10. Conversion of propane (a) and selectivity to methane + ethylene (b), propylene (c), and BTX (d) over the parent HZSM-5 and ALD ZnO modified ZSM-5: (□) HZSM-5, (○) 1c-ZnO-ZSM-5, (△) 2c-ZnO-ZSM-5, (▽) 3c-ZnO-ZSM-5 (T= 550℃, WHSV= 400 h^{-1})

Besides coke formation, other factors such as sintering of the catalytic phase and evaporation of ZnO species may also contribute to the deactivation of ALD ZnO modified zeolites. In order to investigate these factors, after the stability tests the used catalysts were calcined in air at 550℃ for 4hrs to remove the coke species deposited on the catalysts. After the coke removal treatments the activity of 1c-ZnO-ZSM-5 could be completely recovered. Therefore coke formation is indeed the primary reason for the deactivation of ZSM-5 supported ALD ZnO catalyst. However, for 1c-ZnO-Y only ~70% of the original activity could be retained after the coke removal. By comparing the XRD patterns of 1c-ZnO-Y before and after the stability test and the catalyst regeneration, a sharp peak corresponding to the [101] crystal plane of ZnO can be observed at $2\theta=36.4^{o}$ on the regenerated catalyst (Figure S1), implying that highly dispersed ZnO species crystallize during the catalysis test. The used catalyst was also inspected by SEM and small crystals of ZnO can be observed on the surface of the zeolite (Figure S2). ICP measurements indicated that the content of Zn in 1c-ZnO-Y decreased from 11.9% to 11.1% after the catalyst regeneration. Therefore the loss of Zn species due to evaporation of ZnO during the reaction may also contribute to the reduced activity of the regenerated catalyst. Based on these findings we conclude that the deactivation of Y zeolite supported ALD ZnO catalyst is due to the combined effects of coke formation, sintering or crystallization of the catalytic phase, and evaporation of ZnO. Compared to some other metal oxide catalysts supported on zeolites for propane conversion, the deactivations of ALD ZnO catalysts are faster. [55, 56] This is probably related to the high loading of ZnO as a result of the saturated ALD surface reaction. The ALD process produces high-density ZnO sites on the support; this brings about excellent catalytic activity but may also facilitate generation of coke species and crystallization of catalytic phases, which will lead to accelerated deactivation of the catalyst. The future work will focus on improving the stabilities of these ALD ZnO modified zeolites.

Conclusions

Highly dispersed ZnO species modified ZSM-5 and Y zeolites are prepared by performing atomic layer deposition of ZnO to HZSM-5 and HY using diethylzinc and water as the precursors. Substantial amounts of ZnO can be introduced to the zeolites by carrying out ALD under saturated reaction conditions. As revealed by multiple characterization techniques such as weight gain analysis, N_2 physisorption, XRD, SEM, XPS, TPR and TGA, isolated $Zn(OH)^{+}$ species are predominantly formed on both zeolites after the first cycle of ZnO ALD. Because the pore size of HZSM-5 is very close to the diameter of DEZ, the precursor molecules could only enter the micropores during the first ALD cycle; during subsequent ALD cycles the isolated $Zn(OH)^{+}$ species formed in the internal cavities of ZSM-5 almost remain unchanged while bulky Zn_mO_n clusters are gradually formed on the external surface. The

micropore size of Y zeolite is much larger than the diameter of DEZ so that the precursor molecules could infultrate the micropores during the first three cycles of ZnO ALD. Consequently on both internal and external surfaces of Y zeolite the isolated $Zn(OH)^+$ species could be converted to Zn_mO_n clusters. Results from Py-IR characterization suggest that the ALD fabrication to Y zeolite completely eliminates the Brønsted acid sites and greatly increases the number of strong Lewis acid sites. Similar effects are obtained on ALD ZnO modified ZSM-5 except that the Brønsted acid sites on ZSM-5 are only partially removed. In the propane dehydrogenation /aromatization reaction the ALD ZnO modified zeolites exhibit greatly enhanced catalytic activities. Propylene is the major reaction product on ALD ZnO modified Y zeolite and high selectivities to aromatics are achieved on ALD ZnO modified ZSM-5. These results suggest that ZnO species merely promote the dehydrogenation reaction while the subsequent oligomerization and cyclization reactions require Brønsted acid sites. For both zeolites the catalyst modified by only 1 or 2 cycles of ZnO ALD performs better than those modified by multiple cycles of ALD, indicating that isolated $Zn(OH)^+$ species are more effective for the conversion of propane to propylene and aromatics. Despite their impressive initial catalytic performances, deactivations are rather fast for these ALD ZnO modified zeolites. Coke formation is the primary reason for the deactivation of ZSM-5 supported ALD ZnO catalyst. The deactivation of Y zeolite supported ALD ZnO is due to the combined effects of coke formation, sintering or crystallization of the catalytic phase, and evaporation of ZnO.

Acknowledgments

This work is financially supported by National Natural Science Foundation of China (No. 21203146).

References

1 A. Corma, Inorganic Solid Acids and Their Use in Acid-Catalyzed Hydrocarbon Reactions, *Chem. Rev.*, 1995, **95**, 559-614.

2 N. Rahimi and R. Karimzadeh, Catalytic Cracking of Hydrocarbons over Modified ZSM-5 Zeolites to Produce Light Olefins: A review, *Appl. Catal., A: Gen.*, 2011, **398**, 1–17.

3 E. A. Pidko, S. M. T. Almutairi, B. Mezari, P. C. M. M. Magusin and E. J. M. Hensen, Chemical Vapor Deposition of Trimethylaluminum on Dealuminated Faujasite Zeolite, *ACS Catal.*, 2013, **13**, 1504-1517.

4 P. Serp, P. Kalck and F. Roselyne, Chemical Vapor Deposition Methods for The Controlled Preparation of Supported Catalytic Materials, *Chem. Rev.*, 2002, **102**, 3085-3128.

5 J. A. Biscardi and E. Iglesia, Structure and Function of Metal Cations in Light Alkane Reactions Catalyzed by Modified H-ZSM5, *Catal. Today*, 1996, **31**, 207-231.

6 J. A. Biscardi and E. Iglesia, Non-oxidative Reactions of Propane on Zn/Na-ZSM5. *Phys. Chem. Chem. Phys*., 1999, **1**, 5753-5759.

7 J. A. Biscardi, G. D. Meitzner and E. Iglesia, Structure and Density of Active Zn Species in Zn/H-ZSM5 Propane Aromatization Catalysts, *J. Catal*., 1998, **179**, 192-202.

8 J. A. Biscardi and E. Iglesia, Reaction Pathways and Rate-Determining Steps in Reactions of Alkanes on H-ZSM5 and Zn/H-ZSM5 Catalysts, *J. Catal*.**,** 1999, **182**, 117-128.

9 X. J. Niu, J. Gao, Q. Miao, M. Dong, G. F. Wang, W. B. Fan, Z. F. Qin and J. G. Wang, Influence of Preparation Method on The Performance of Zn-containing HZSM-5 Catalysts in Methanol-to-aromatics, *Microporous Mesoporous Mater.*, 2014, **197**, 252-261.

10 Y. M. Ni, A. M. Sun, X. L. Wu, G. L. Hai, J. L. Hu, T. Li and G. X. Li, The Preparation of Nano-sized H[Zn, Al]ZSM-5 Zeolite and Its Application in The Aromatization of Methanol, *Microporous Mesoporous Mater.*, 2011, **143**, 435-442.

11 Z. H. Fu, D. L. Yin, Y. S. Yang and X. X. Guo, Characterization of Modified ZSM-5 Catalysts for Propane Aromatization Prepared by A Solid State Reaction, *Appl. Catal., A: Gen.*, 1995, **124**, 59-71.

12 S. Tamiyakul, W. Ubolcharoen, D. N. Tungasmita and S. Jongpatiwut, Conversion of Glycerol to Aromatic Hydrocarbons over Zn-promoted HZSM-5 Catalysts, *Catal. Today.*, 2015, *In Press*.

13 S. M. T. Almutairi, B. Mezari, P. C. M. M. Magusin, E. A. Pidko and E. J. M. Hensen, Structure and Reactivity of Zn-Modified ZSM-5 Zeolites: The Importance of Clustered Cationic Zn Complexes, *ACS Catal*, 2012, **2**, 71-83.

14 P. L. D. Cola, R. Gläser and J. Weitkamp, Non-oxidative Propane Dehydrogenation over Pt-Zn-containing Zeolites, *Appl. Catal., A: Gen*, 2006, **306**, 85-97.

15 H. Berndt, G. B. Lietz and L. J. Völter, Zinc Promoted H-ZSM-5 Catalysts for Conversion of Propane to Aromatics Ⅰ. Acidity and Activity, *Appl. Catal., A: Gen*, 1996, **146**, 351-363.

16 V. B. Kazansky, A. I. Serykh and E. A. Pidko, DRIFT Study of Molecular and Dissociative Adsorption of Light Paraffins by HZSM-5 Zeolite Modified with Zinc Ions: Methane Adsorption, *J. Catal.*, 2004, **225**, 369-373.

17 V. B. Kazansky, A. I. Serykh, B. G. Anderson and R. A. V. Santen, The Sites of Molecular and Dissociative Hydrogen Adsorption in Highsilica Zeolites Modified with Zinc Ions. III DRIFT Study of H_2 Adsorption by The Zeolites with Different Zinc Content and Si/Al Ratios in The Framework, *Catal. Lett.*, 2003, **88**, 3-4.

18 V. B. Kazansky, V. Y. Borovkov, A. I. Serikh, R. A. V. Santen and B. G. Anderson, Nature of The Sites of Dissociative Adsorption of Dihydrogen and Light Paraffins in ZnHZSM-5 Zeolite Prepared by Incipient Wetness Impregnation, *Catal. Lett.*, 2000, **66**, 39-47.

19 V. B. Kazansky, A. I. Serykh, R. A. V. Santen and B. G. Anderson, On The Nature of The Sites of Dihydrogen Molecular and Dissociative Adsorption in ZnHZSM-5 .II. Effects of Sulfidation, *Catal. Lett.*, 2001, **74**, 1-2.

20 B. J. O'Neill, D. H. K. Jackson, J. Lee, C. Canlas, P. C. Stair, C. L. Marshall, J. W. Elam, T. F. Kuech, J. A. Dumesic and G. W. Huber, Catalyst Design with Atomic Layer Deposition, *ACS Catal*, 2015, **5**, 1804-1825.

21 H. Feng, J. W. Elam, J. A. Libera, W. Setthapun and P. C. Stair, Palladium Catalysts Synthesized by Atomic Layer Deposition for Methanol Decomposition, *Chem. Mater.*, 2010, **22**, 3133-3142.

22 S. T. Christensen, H. Feng, J. A. Libera, G. Neng, J. T. Miller, P. C. Stair and J. W. Elam, Supported Ru-Pt Bimetallic Nanoparticle Catalysts Prepared by Atomic Layer Deposition, *Nano Lett.*, 2010, **10**, 3047-3051.

23 H. Feng, J. A. Libera, P. C. Stair, J. T. Miller and J. W. Elam, Subnanometer Palladium Particles Synthesized by Atomic Layer Deposition, *ACS Catal*, 2011, **1**, 665-673.

24 H. Feng, J. Lu, P. C. Stair and J. W. Elam, Alumina over-coating on Pd Nanoparticle Catalysts by Atomic Layer Deposition: Enhanced Stability and Reactivity, *Catal. Lett.*, 2011**, 141**, 512-517.

25 H. Feng, J. W. Elam, J. A. Libera, M. J. Pellin and P. C. Stair, Oxidative Dehydrogenation of Cyclohexane over Alumina-supported Vanadium Oxide Nanoliths, *J. Catal.*, 2010**, 269**, 421-431.

26 L. J. Qin, T. Gong, H. X. Hao, K. Y. Wang and H. Feng, Core-shell-structured Nanothermites Synthesized by Atomic Layer Deposition, *J. Nanopart. Res.*, 2013, **15**, 2150-2165.

27 T. Gong, L. J. Qin, W. Zhang, H. Wan, J. Lu and H. Feng, Activated Carbon Supported Palladium Nanoparticle Catalysts Synthesized by Atomic Layer Deposition: Genesis and Evolution of Nanoparticles and Tuning The Particle Size, *J. Phys. Chem. C*, 2015, **119**, 11544-11556.

28 E. Rikkinen, A. Santasalo-Aarnio, S. Airaksinen, M. Borghei, V. Viitanen, J. Sainio, E. I. Kauppinen, T. Kallio and A. O. I. Krause, Atomic Layer Deposition Preparation of Pd Nanoparticles on A Porous Carbon Support for Alcohol Oxidation, *J. Phys. Chem. C*, 2011, **115**, 23067-23073.

29 S. P. Sree, J. Dendooven, J. Jammaer, K. Masschaele, D. Deduytsche, J. D'Haen, C. E. A. Kirschhock, J. A. Martens, and C. Detavernier, Anisotropic Atomic Layer Deposition Profiles of TiO_2 in Hierarchical Silica Material with Multiple Porosity, *Chem. Mater.*, 2012, **24**, 2775-2780.

30 J. L. Lu, J. W. Elam and P. C. Stair, Synthesis and Stabilization of Supported Metal Catalysts by Atomic Layer Deposition, *Acc. Chem. Res.*, 2013, **8**, 1806-1815.

31 S. P. Sree, J. Dendooven, T. I. Kora´nyi, G. Vanbutsele, K. Houthoofd, D. Deduytsche, C. Detavernier and J. A. Martens, Aluminium Atomic Layer Deposition Applied to Mesoporous Zeolites for Acid Catalytic Activity Enhancement, *Catal. Sci. Technol.*, 2011, **1**, 218-221.

32 J. W. Elam, J. A. Libera, T. H. Huynh, H. Feng and M. J. Pellin, Atomic Layer Deposition of Aluminum Oxide in Mesoporous Silica Gel, *J. Phys. Chem. C*, 2010, **114**, 17286-17292.

33 H. Vuori, R. J. Silvennoinen, M. Lindblad, H. Österholm and A. O. I. Krause, Beta Zeolite-supported Iridium Catalysts by Gas Phase Deposition, *Catal. Lett.*, 2009, **131**, 7-15.

34 B. D. Vandegehuchte, J. W. Thybaut, C. Detavernier, D. Deduytsche, J. Dendooven, J. A. Martens, S. P. Sree, T. I. Korányi and G. B. Marin, A Single-Event MicroKinetic Assessment of N-alkane Hydroconversion on Ultrastable Y Zeolites after Atomic Layer Deposition of Alumina, *J. Catal.*, 2014, **311**, 433-446.

35 H. Feng, J. W. Elam, J. A. Libera, M. J. Pellin and P. C. Stair, Catalytic Nanoliths, *Chem. Eng. Sci.*, 2009, **64**, 560-567.

36 J. W. Elam, G. M. Groner and S. M. George, Viscous Flow Reactor with Quartz Crystal Microbalance for Thin Film Growth by Atomic Layer Deposition, *Rev. Sci. Instrum.*, 2002, **73**, 2981-2987.

37 O. Sneh, M. L. Wise, A. W. Ott, L. A. Okada and S. M. George, Atomic Layer Growth of SiO_2 on Si(100) Using $SiC1_4$ and H_2O in A Binary Reaction Sequence, *Surf. Sci.*, 1995, **334**, 135-152.

38 M. A. Cameron, I. P. Gartland, J. A. Smith, S. F. Diaz and S. M. George, Atomic Layer Deposition of SiO_2 and TiO_2 in Alumina Tubular Membranes: Pore Reduction and Effect of Surface Species on Gas Transport, *Langmuir*, 2000, **16**, 7435-7444.

39 Y. Du, X. Du and S. M. George, SiO_2 Film Growth at Low Temperatures by Catalyzed Atomic Layer Deposition in A Viscous Flow Reactor, *Thin Solid Films*, 2005, **491**, 43-53.

40 C. L. Bowes, A. Malek and G. A. Ozin, Chemical Vapor Deposition Topotaxy in Porous Hosts, *Chem. Vap. Deposition*, 1996, **2**, 97-103.

41 D. L. Lu, J. N. Kondo, K. Domen, H. A. Begum and M. Niwa, Ultra-fine Tuning of Microporous Opening Size in Zeolite by CVD, *J. Phys. Chem. B*, 2004, **108**, 2295-2299.

42 These data can be obtained from The Cambridge Crystallographic Data Centre via www.ccdc.cam.ac.uk/data_request/cif.

43 B. Li, S. J. Li, N. Li, H. Y. Chen, W. J. Zhang, X. H. Bao and B. X. Lin, Structure and Acidity of Mo/ZSM-5 Synthesized by Solid State Reaction for Methane Dehydrogenation and Aromatization,

Microporous Mesoporous Mater., 2006, **88**, 244-253.

44 Y. W. Zhang, Y. M. Zhou, H. Liu, Y. Wang, Y. Xu and P. C. Wu, Effect of La Addition on Catalytic Performance of PtSnNa/ZSM-5 Catalyst for Propane Dehydrogenation, *Appl. Catal., A: Gen*, 2007, **333**, 202-210.

45 S. B. Zhang, Y. M. Zhou, Y. W. Zhang and L. Huang, Effect of K Addition on Catalytic Performance of PtSn/ZSM-5 Catalyst for Propane Dehydrogenation, *Catal. Lett.*, 2010, **135**, 76-82.

46 D. F. Jin, B. Zhu, Z. Y. Hou, J. H. Fei, H. Lou and X. M. Zheng, Dimethyl Ether Synthesis via Methanol and Syngas over Rare Earth Metals Modified Zeolite Y and Dual Cu-Mn-Zn Catalysts, *Fuel*, 2007, **86**, 2707-2713.

47 A. G. Popov, A. V. Smirnov, E. E. Knyazeva, V. V. Yuschenko, E. A. Kalistratova, K. V. Klementiev, W. Grünert and I. I. Ivanova, Ni-, Co-, Fe- and Zn-containing Silicalites-1 in Propane Conversion, *Microporous Mesoporous Mater.*, 2010, **134**, 124-133.

48 F. L. Liao, Y. Q. Huang, J. W. Ge, W. R. Zheng, K. Tedsree, P. Collier, X. L. Hong and S. C. Tsang, Morphology-dependent Interactions of ZnO with Cu Nanoparticles at The Materials' Interface in Selective Hydrogenation of CO_2 to CH_3OH, *Angew. Chem. Int. Ed.*, 2011, **50**, 2162-2165.

49 S. W. Park, O. S. Joo, K. D. Jung, H. Kim and S. H. Han, Development of ZnO/Al_2O_3 Catalyst for Reverse-water-gas-shift Reaction of CAMERE (Carbon Dioxide Hydrogenation to Form Methanol via A Reverse-water-gas-shift reaction) Process, *Appl. Catal., A: Gen*, 2001, **211**, 81-90.

50 N. S. Gnep, J. Y. Doyemet, A. M. Seco, F. R. Ribeiro and M. Guisnet, Conversion of Light Alkanes to Aromatic Hydrocarbons II. Role of Gallium Species in Propane Transformation on GaHZSM5 Catalysts, *Appl. Catal.*, 1988, **43**, 155-166.

51 M. Guisnet, N. S. Gnep and F. Alario, Aromatization of Short Chain Alkanes on Zeolite Catalysts, *Appl. Catal., A: Gen*, 1992, **89**, 1-30.

52 A. A. Gabrienko, S. S. Arzumanov, A. V. Toktarev, I. G. Danilova, D. Freude and A. G. Stepanov, H/D Exchange of Molecular Hydrogen with Brønsted Acid Sites of Zn- and Ga-modified Zeolite BEA. *Phys. Chem. Chem. Phys.*, 2010, **12**, 5149-5155.

53 A. G. Stepanov, S. S. Arzumanov, A. A. Gabrienko, A. V. Toktarev, V. N. Parmon and D. Freude, Zn-promoted Hydrogen Exchange for Methane and Ethane on Zn/H-BEA Zeolite: In Situ ^{1}H MAS NMR Kinetic Study, *J. Catal.*, 2008, **253**, 11-21.

54 A. A. Gabrienko, S. S. Arzumanov, D. Freude and A. G. Stepanov, Propane Aromatization on Zn-Modified Zeolite BEA Studied by Solid-State NMR in Situ, *J. Phys. Chem. C*, 2010, **114**, 12681–12688.

55 Y. J. Ren, F. Zhang, W. M. Hua, Y. H. Yue and Z. Gao, ZnO Supported on High Silica HZSM-5 as New Catalysts for Dehydrogenation, *Catal. Today.*, 2009, **148**, 316-322.

56 J. J. Guo, H. Lou, H. Zhao, L. H. Zheng and X. M. Zheng, Dehydrogenation and Aromatization of Propane over Rhenium-modified HZSM-5 Catalyst, *J. Mol. Catal. A: Chem.*, 2005, **239**, 222-227.